Tridimensional image reconstruction method based on the modified algebraic reconstruction technique and B-spline interpolation

Gilmar Cação Ribeiro[1]
Paulo Estevão Cruvinel[2]

[1]UFSCar-Universidade Federal de São Carlos- Departamento de Computação
Rodovia Washington Luis, Km235, 13565-905, São Carlos,SP,Brasil
cacao@cnpdia.embrapa.br

[2]EMBRAPA-CNPDIA- Empresa Brasileira de Pesquisa Agropecuária
Rua XV de Novembro 1452, Caixa Postal 741 , 13560-970, São Carlos,SP, Brasil
cruvinel@cnpdia.embrapa.br

Abstract . This study presents an algorithm for three-dimensional reconstruction of tomographic images based on reconstructed two-dimensional slices, using a modification of the technique of additive algebraic reconstruction and the spline function for interpolation of the intermediary planes in volumetric reconstruction. Development of the method was first destined to image reconstruction of the minitomographer at the National Center for Research and Instrumentation Development for Agriculture (CNPDIA) of the Brazilian Agricultural Research Company (EMBRAPA), which is dedicated to soil science. Evaluation of the results of the method was based on phantom images and soil samples, with 2mm spatial resolution, 60 samples per projection, a 3 degree angle between projections, a 59.9 KeV Americium (^{241} Am) energy source, and a ten-second time per projection sample. The results prove the usefulness and reliability of the method, which is also applicable to other tomographic systems.

Keywords : minitomographer, tomography, 3-D image reconstruction.

1- Introduction

Over the past few decades, computerized tomography has been increasingly employed as a very useful technique in multidisciplinary applications, ranging from modern medicine using X-ray computerized tomography (CT) and Nuclear Magnetic Resonance (NMR) to the study of materials such as soils.

In 1917, J. Radon [Radon(1917)], for the first time, hit upon a formula for this calculation, which became known as the "Radon Transformed". But it was only in 1921 that Bocage [Bocage (1921)] introduced conventional tomography, or the focal X-ray transmission plan. In 1963, the physicist A. M. Cormack [Cormack(1963,1964)] made a decisive contribution to computerized tomography. These results led to the development, in 1973, of the first commercial tomographer, built by engineer G. N. Hounsfield [Hounsfield (1968,1973)].

With the advent of microelectronics, which led to the production of microcomputers with large memory storage capacity and fast data processing, as well as the development of increasingly sensitive detectors and high precision, low cost electronic components, it became possible to develop computerized tomographers dedicated to specific applications. Tomography by X-ray or γ-ray transmission, in particular, in addition to its applications in the field of medicine, has been used extensively in studies in the field of soil physics [Crestana et al. (1986)], [Cruvinel(1987)], [Vaz et al.(1989)], [Cruvinel et al. (1990)], [Cruvinel--Crestana (1996)].

In conventional tomographic processes, a given section of the body being studied is presented as a map of two-dimensional linear attenuation coefficients which depends on several parameters, such as radiation energy, chemical composition and material density of the body under tomographical study [Hendee (1983)], which furnishes quantitative information regarding the body's material density and qualitative information regarding its form.

Tomography has made great breakthroughs over a short period of time. These breakthroughs involve reduced time for acquisition of data, for reconstruction, and improved image quality. More recently, improve-

ments have involved aspects of contrast, reduced noise, and determination of the attenuation coefficient.

Although each of these factors is important, this work proposes a method for the reconstruction of 3D images that optimizes time in data acquisition and image reconstruction by means of a reduced number of tomographies. The images of these tomographies are reconstructed using the Algebraic Reconstruction Technique introduced by Gordon, Bender and Herman [Gordon--Bender--Herman (1970)], [Gordon--Herman (1971)], [Gordon (1973)], [Herman (1973)], [Gordon (1974)] and, by means of spline interpolation, intermediary slices of the tomographies are created, forming a set of 2D images that are then piled up, forming the final 3D image of the object under study.

The use of interpolation to create intermediary sections of the tomographies is necessary when the tomographies made of the object being studied are not continuous, that is, when there is a space between each tomographic image that would allow for the insertion of one or more additional images. Thus, the creation of interpolated planes serves to provide continuity to the image, without spaces being left between the 3D image slices.

Section 2 presents the basic principle of the algebraic reconstruction technique with its fundamental equations, where the reconstruction plane is discretized in a matrix (nxm) shown in figure 1, and the material used for this work, i.e. the minitomographer and the phantom. Section 3 presents the modified ART algorithm proposed for the reconstruction of 2D images. Section 4 gives the definition and use of the spline function. The results of this study are presented in section 5, showing the images and their histograms. Section 6 presents a quantitative analysis of the results by means of histograms, while our conclusions are presented in section 7.

2 - Materials and methods

The method of algebraic reconstruction was first introduced in 1970 by Gordon et al. During the 70s several other studies based on the algebraic reconstruction technique were also developed [Gordon--Herman(1971), Gordon(1973), Gordon(1974)]. The method for algebraic reconstruction of images is based on a reconstruction space (R), which is divided into a finite number of R_i (i = 1,2,..., n) elements to each of which an f_i density is associated. The distribution of unknown densities is approximated by the values determined by the reconstruction algorithm for each element. It is assumed that the density function is equal to zero outside of the R reconstruction space. Figure 1 illustrates the reconstruction space. The points in the reconstruction space illustrate the $\vec{r}_i$ centroids attributed to each R_i element.

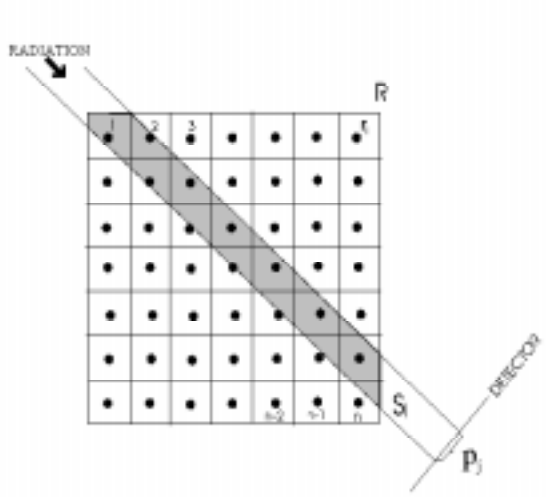

Figure 1- The two-dimensional R reconstruction space with the Radiation-Radius-Detector set.

Radiation incides on a detector, furnishing a p_j measurement which will compose an element of the P_j projection at a given θ angle. This radiation goes through the object by an S_j path, that is represented in figure 1 by the shadowed area. In this particular case radiation runs through the R space in parallel rays at a θ angle and the width of the radius is determined by the opening of the rays' collimators.

Effective interaction between the radiation rays and the R_i elements is schematically presented by the intersection between the S_j path of the ray and the R_i elements, represented by $S_j \cap R_i$.

In the algebraic reconstruction method it is also assumed that each projection is divided into m non-superimposed projection elements (p_j , j=1,2,…,m). The behavior of S_j in R depends on the angle of projection. Thus, since $\vec{r}$ represents a centroid in R and $f(\vec{r})$ represents the unknown density function in $\vec{r}$, then:

$$\int_{S_j} f(\vec{r})\, d\vec{r} \approx p_j \qquad \text{for } j=1,2,...,m \qquad \text{(I)}$$

where p_j is the experimental measure of the j-th element of the $f(\vec{r})$ projection. The "≈" sign indicates that the measuring process is not exact.

Thus, a projection element p_j of the projection at angle θ will be given by:

$$p_j \approx \sum_i \int_{S_j \cap R_i} f(\vec{r})\, d\vec{r} \quad \text{for} \quad \begin{matrix} j=1,2,...,m \\ i=1,2,...,n. \end{matrix} \qquad \text{(II)}$$

An approximation for the unknown density function $f(\vec{r})$ is obtained by determining the f_i values

for each R_i region. The best estimate results when f_i is the mean value of $f(\vec{r})$ over the R_i region, that is:

$$f_i = \frac{\int_{R_i} f(\vec{r})\, d\vec{r}}{\int_{R_i} d\vec{r}} \qquad \text{for } i=1,2,...,n \qquad \text{(III)}$$

With the algebraic reconstruction method, an exact result for the densities cannot be reached due to the limited number of tomographic projections, because of data degeneration during the process of acquisition and tomographic sweeping, and due to the reconstruction algorithm's iterative characteristics.

Because the $f(\vec{r})$ function varies over the R_i region, particularly for heterogeneous objects, its value in $S_j \cap R_i$ is unknown. However, one can presume, by the best estimates, that f_i is the mean value of $f(\vec{r})$ over R_i, so the integral over $S_j \cap R_i$ can be estimated by the geometric fraction presented in equation (III), being given by:

$$w_{ij} = \frac{\int_{S_j \cap R_i} d\vec{r}}{\int_{R_i} d\vec{r}} \qquad \begin{matrix} \text{for } i=1,2,...,n \\ j=1,2,...,m \end{matrix} \qquad \text{(IV)}$$

multiplied by f_i , that is :

$$\int_{S_j \cap R_i} f(\vec{r})\, d\vec{r} \approx w_{ij} f_i \qquad \begin{matrix} \text{for } i = 1,2,...n \\ j=1,2,...,m \end{matrix} \qquad \text{(V)}$$

where w_{ij} is the portion (or part) of the R_i area intercepted by the path of the S_j ray in relation to the total area of the R_i element. It thus follows that equation (II) becomes a set of linear equations of the unknown f_i , that is:

$$\begin{cases} p_1 \approx w_{11} f_1 + w_{21} f_2 + \cdots + w_{n1} f_n \\ p_2 \approx w_{12} f_1 + w_{22} f_2 + \cdots + w_{n2} f_n \\ \vdots \\ p_m \approx w_{1m} f_1 + w_{2m} f_2 + \cdots + w_{nm} f_n \end{cases} \qquad \text{(VI)}$$

To evaluate the method, tomographic phantom images and soil samples were obtained with the minitomographer developed by CNPDIA-EMBRAPA. This minitomographer uses X-ray and γ-ray as sources of radiation [Cruvinel(1987), Cruvinel et al. (1990)]. The hardware has a mechanical table, an X-ray or γ-ray emission source, 2 collimators with variable size windows, a cristal detector of the NaI(Tl) type, an electronic pulse counter, an electronic processing system for nuclear measures and a microcomputer.

The time required for data acquisition depends on the size of the sample, the desired resolution, and the equipment's precision. This experiment used 2mm spatial resolution, 60 samples per projection, an angle of 3° between projections, a 59.9 KeV Americium (^{241} Am) energy source, and a preset time of 10 seconds per projection sample.

Figure 2 shows a conceptual drawing of the diagram of the phantom used to evaluate the method. The phantom is non-symmetrical and non-homogeneous, containing three different densities related to the Aluminum (Al), Calcium (Ca) and SiO_2 elements. For this study, 6 two-dimensional tomographies (S3, S4, S5, S6, S7, S8) were made and 3 planes (S34, S45, S78) per spline interpolation were generated.

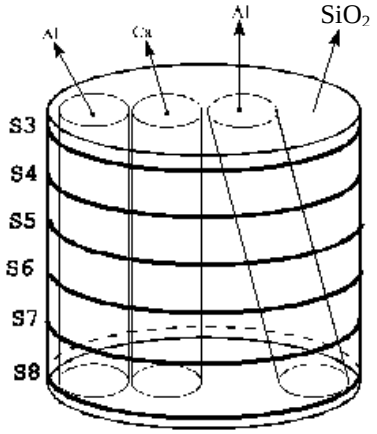

Figure 2 - Phantom with different attenuation coefficients and slices.

3 - The modified ART algorithm (ARTAM)

The algebraic reconstruction algorithm developed for this work has a function, called a correction factor, which is used to determine the area that each ray intercepts in the reconstruction matrix. Each ray does not always intercept every element of R_i reconstruction and, for that reason, only the value of the part that is intercepted by the ray was taken. This happens in the case of all the ray's elements, except for the 0°, 90°, and 180° angles. The ray's correction factor (Fc) is calculated taking into consideration the area that intercepts it in the R reconstruction space (AR), the area of a reconstruction element (Aler) and the number of reconstruction elements contained in the ray (Nel), given by:

$$Fc = \frac{AR}{(A1er)(Nel)} \qquad \text{(VII)}$$

Operation of the algorithm is started using an initial estimate for the solution. This initial estimate for the solution will be constant and equal for all the f_i.

Defining the initial estimate as f_i^0 for the solution and f_i^q the q-th estimate after q iterations, this will be given by :

$$f_i^0 = \bar{f} = \frac{\sum_{j=1}^{m} p_j}{n} \qquad \text{(VIII)}$$

where *n* is the number of reconstruction elements in the R space and m is the number of rays per projection.

Once the initial estimates are given, the algorithm will find the next estimates in the following manner:

$$f_i^{(q+1)} = \max\left\{0, f_i^{(q)} + \left(\frac{p_j - \left[(Fc)(p_j^q)\right]}{N_j}\right)\right\} \qquad \text{(IX)}$$

i such that $\vec{r}_i \in s_j$, j=1+mod$_m$q and q=0,...,Km- 1.

In equation (IX), p_j^q is the sum of the reconstruction elements representing the S_j path after q iterations, the "max" function finds the maximum value between two values so that f_i is always positive, the mod$_m$ function calculated the rest of the division of q by m, K is the number of projections and N_j is the number of reconstruction elements that the j ray intercepts in the R reconstruction space.

In each iteration, the difference is calculated between the data obtained for an element of measured projection (p_j) and the sum of the reconstruction elements that it represents (p_j^q). The correction is divided uniformly by the N_j reconstruction elements contained in the S_j path and added to the previous estimate.

The calculation is repeated for the set of projection elements until the result converges toward a reasonable solution. In this study, assurance of convergence was reached by using the criterium for convergence by discrepancy between the measured and calculated projection elements, which optimizes machine time and provides easy implementation. The criterium for convergence by discrepancy is reached using equation (X), that is:

$$D^q = \sqrt{\frac{1}{m}\sum_{j=1}^{m}\left(\frac{\left[p_j - \left[(Fc)(p_j^q)\right]\right]^2}{N_j}\right)} \qquad \text{(X)}$$

where q is the number of the iteration, m is the number of projection rays, N_j is the number of reconstruction elements contained in the S_j path, p_j is the value of a projection element measured on the minitomographer, Fc is the correction factor and p_j^q is the sum of the reconstruction elements representing the S_j path after q iterations.

4 - The B-spline

In addition to the 2D reconstruction method with the modified algebraic reconstruction technique, the B-spline technique was used in order to obtain planes intermediary to those obtained by tomography.

The B-spline is a mathematical technique for modeling curves and surfaces. It is formed by parts of a polynomial that is segments of continuous curves and these segments are united by points called nodes, approximating the control points P_0 throught P_m.

The B-spline offers the advantages of exerting local control over the curve, that is, when a value is altered, only the points near this value are altered.

The curve segments are defined by a set of blending functions that are dependent on the interval between the node values and are defined alternatively according to the blending functions of minor order.

The general formula of the B-spline [Farin (1990)] is given by equation (XI), i.e.:

$$p(t) = \sum_{i=0}^{m} P_i N_{i,k}(t) \qquad \text{(XI)}$$

where p(t) is the polynomial of the B-spline, P_i is the i-th control point, $N_{i,k}$ is the blending function considered and k is the order of blending function.

The blending functions can be defined, alternatively, by:

$$N_{i,1} = \begin{cases} 1 & \text{se } t_i \le t < t_{i+1} \\ 0 & \text{caso contrario} \end{cases} \qquad (t_0 \le t \le t_{m+k}) \qquad \text{(XII)}$$

where the t parameter takes on values in the $[t_0 , t_{m+k}]$ interval and (m+1) is the number of control points. In the B-spline technique, the subsequent blending functions are defined recursively as :

$$N_{i,k}(t) = \frac{(t - t_i)}{t_{i+k-1} - t_i} N_{i,k-1}(t) + \frac{(t_{i+k} - t)}{t_{i+k} - t_{i+1}} N_{i+1,k-1}(t) \qquad \text{(XIII)}$$

where $N_{i,k}$ is the blending function of k order for the P_i control point. The node values $[t_0 , t_{m+k}]$ are chosen following the rule below:

$$\begin{aligned} t_i &= 0 && \text{if } i < k \\ t_i &= i-k+1 && \text{if } k<i<m \quad t \in [0 , m-k+2] \\ t_i &= m-k+2 && \text{if } i > m \end{aligned} \qquad \text{(XIV)}$$

The B-spline takes, as points in each image, the values of the coefficients that have the same coordinates (x,y) in the matrix images and aproximate them. In this way values are obtained for intermediary planes to the planes obtained experimentally.

5 - Results

Figure 3 shows the 2D images of the reconstruction by the ARTAM algorithm and images of the planes generated B-spline.

Figure 4 illustrates the histograms with their respective Gauss curves of the figure 3 images. Table 1 supplies the parameters of the Gauss curve of the reconstructed and interpolated images, where Chi^2 is the difference between the value of the Gauss curve and the real value of the image histogram, the center of the Gauss curve indicates the mean value of the image attenuation coefficients and the standard deviation indicates the mean deviation from the center of the Gauss curve.

S34 is the image generated by the B-spline between images S3 and S4, S45 is the image generated by the B-spline between images S4 and S5 and S78 is the image generated by the B-spline between images S7 and S8.

Image	Chi^2	Gauss Center	Standard deviation
S3	2095.56	52.69 ± 0.47	13.40 ± 0.94
S34	1282.17	52.57 ± 0.39	13.19 ± 0.80
S4	1906.33	52.61 ± 0.44	13.53 ± 0.88
S45	1070.54	52.54 ± 0.34	12.87 ± 0.69
S5	1774.66	52.58 ± 0.41	13.30 ± 0.84
S7	1928.39	52.67 ± 0.36	11.49 ± 0.72
S78	1158.33	52.63 ± 0.28	10.69 ± 0.56
S8	1939.22	52.73 ± 0.36	11.69 ± 0.73

Table 1 - Parameters of the Gauss curve of the image histograms

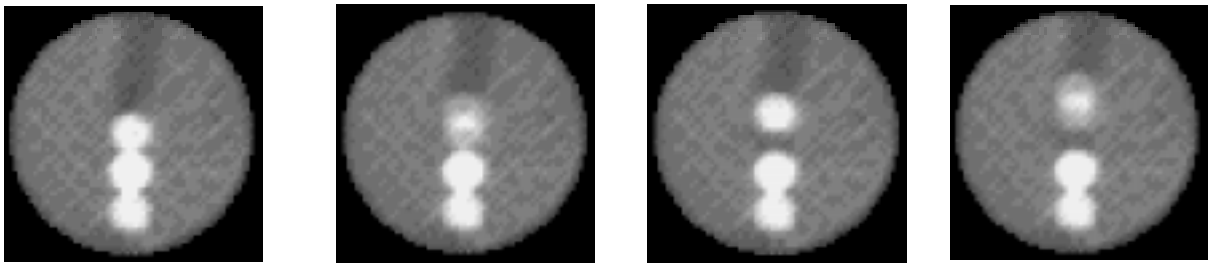

(a) S3 (b) S34 (c) S4 (d) S45

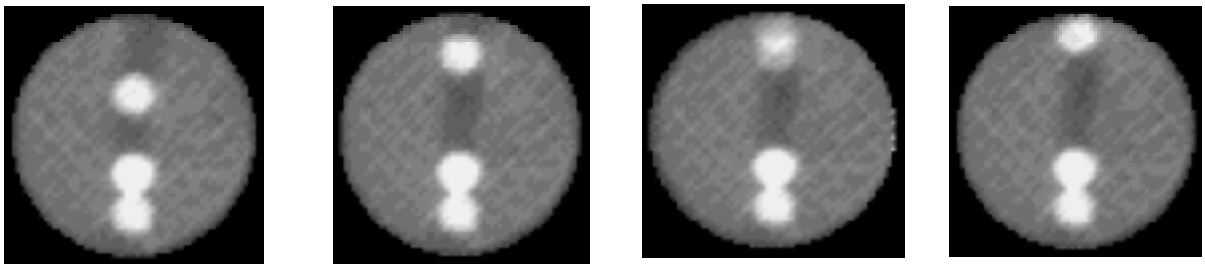

(e) S5 (f) S7 (g) S78 (h) S8

Figure 3 - Images reconstructed by ARTAM (a,c,e,f,h) and images generated by B-spline (b,d,g).

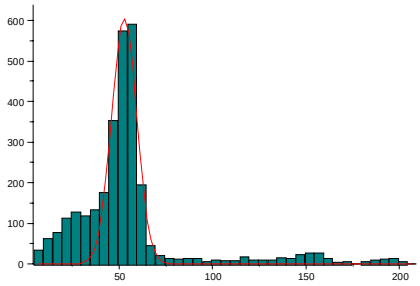

(a) S3

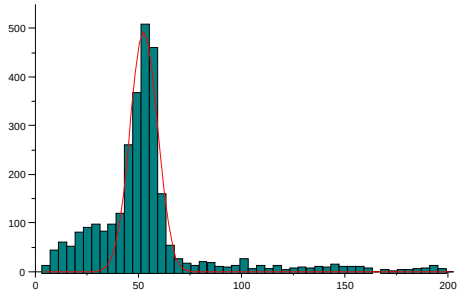

(b) S34

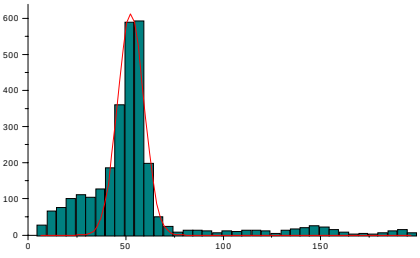

(c) S4

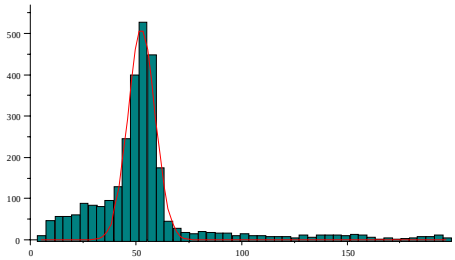

(d) S45

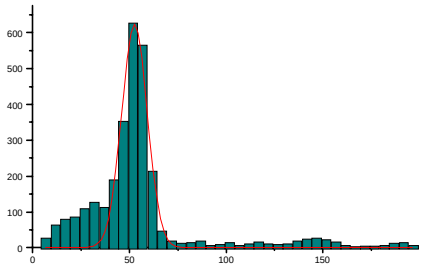

(e) S5

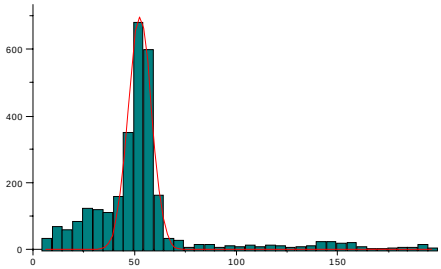

(f) S7

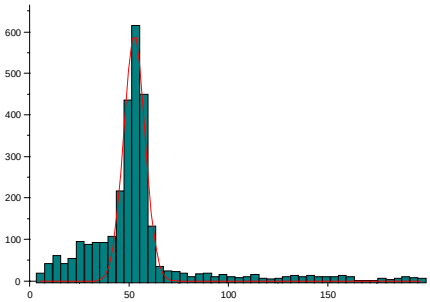

(g) S78

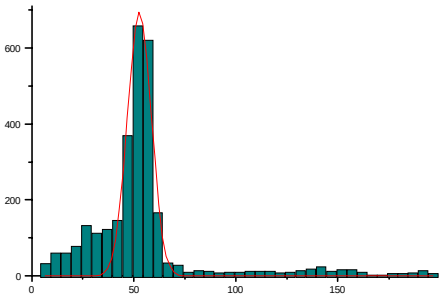

(h) S8

Figure 4 - Histograms (frequency of ocorrency versus linear attenuation coeficients in 1000/cm) of the images reconstructed by ARTAM (a,c,e,f,h) and the images obtained by B-spline (b,d,g)

6 - Analysis of the results

The results are analyzed quantitatively by means of the Gauss curve parameter histograms, since the histograms furnish a quantitative description of the appearance of each image or plane.

An analysis of the value of the Chi^2 parameter in table 1 shows a significant variation between the values of the reconstructed images and those of the interpolated ones. This is due to the non-symmetry and non-homogeneity of the phantom, since the points of each image taken as the point of interpolation have different values, resulting in a coefficient value that is intermediary to them at the point generated at the interpolation.

Observing table 1 it can be noted that the center of the Gauss curve has a very small variation of around 0.25. In this case, the standard deviation was also subject to a small variation. This happened because the phantom is non-homogeneous and non-symmetrical. Thus, it was to be expected that there would be some variation in the image's quantitative and qualitative data, as can be seen in the histograms and images of figure 3.

In the interpolation, when only one plane is generated between the interpolated images, it can be seen, from table 1, that the standard deviation of the images is subject to a very small variation in relation to the images used in the interpolation. Analyzing the results of the phantom one can see a distortion in the region relative to the attenuation coefficient of the Silica due to the non-symmetry of the phantom, and it is because of this non-symmetry that the attenuation coefficients are the same at only a few of the points. In the other areas where the coefficients are not the same a coefficient value is produced that is intermediary to the values of the images used in the interpolation, which was already expected. Even so, however, the result obtained is considered satisfactory and the image resulting from the interpolation presents a good quantitative result.

It can be seen, from figure 3, that the images obtained through interpolation show less contrast than the images reconstructed by means of the method presented in this study. This method also presents some border effects which are stronger in the images generated by interpolation. This effect is caused by the large difference between the levels of gray of the areas, but it can be reduced through appropriate techniques.

It was noted in this study that the more planes are generated by interpolation between every two images reconstructed by ARTAM, the better are the quantitative and qualitative results of the images generated.

7 - Conclusion

This study shows that it is feasible to use the ARTAM algorithm and the Spline function for 3D tomographic image reconstruction in the minitomographer dedicated to agriculture. There are solutions for the algorithm's limitations according to specific applications, such as, for example, the use of filters to improve the image and by producing tomographic splices close to each other in order to avoid excessive distortion of the interpolated image. The 3D reconstruction algorithm employed is useful in the sense that it optimizes reconstruction and image acquisition time, since, by using interpolation, the time spent on the tomography is reduced to one half or even less, depending on the number of images one wants to produce through interpolation between each splice obtained tomographically.

8 - Acknowledgments

The authors wish to acknowledge the support offered by the EMBRAPA-CNPDIA, Department of Computer Science of the Federal University of São Carlos, CNPq and project AVVIC (680.063/95-1 and 481023/96.8) .

9 - References

CORMACK, A. M. ; "Representation of a Function by Its Line Integrals with some Radiological Applications", J. Appl. Physics 34(9) (1963), 2722-2727.

CORMACK, A.M.; "Representation of a function by its line integrals with some radiological applications II", J. Appl. Phys. 35 (1964) , 2908-2913.

CRESTANA, S.; CESAREO, R; MASCARENHAS, S.; "Using a computed tomography miniscanner in soil science", Soil Science 142 (1986), n. 1, 56-61.

CRUVINEL, P.E. ; "Minitomógrafo de Raio X e Raio γ Computadorizado para Aplicações Multidisciplinares", Campinas, UNICAMP , 325 p., 1987(Tese Doutorado).

CRUVINEL, P.E ;CESAREO, R; CRESTANA, S.; MASCARENHAS, S. **;** "X and Gama-Ray Computerized Minitomography Scanner for Soil Science", IEEE Transactions on Instrumentation and Measurement 39 (1990)**,** n. 5 , 745-750.

CRUVINEL, P. E., CRESTANA, S.; "Oportunities and use of Digital Signal Processors in Tomography scanners dedicated to agriculture", Workshop Brasileiro de Arquiteturas Alternativas Usando DSP's (1996), São Carlos-SP, 93-97.

FARIN, G.; “Curves and Surfaces for Computer Aided Geometric Design”, San Diego: Academic Press, 1990.

GORDON, R. ; BENDER, R. ; HERMAN, G. T. ; “Algebric Reconstruction Techniques (ART) for Three-dimensional Electron Microscopy and X-ray Photography”, Journal theor. Biol**.** 29 (1970), 471-481.

GORDON, R ; HERMAN, G.T. ; “Reconstruction of Pictures from their projections”, Comm. A.C.M 14 (1971), 759-768.

GORDON, R.;“Artifacts in Reconstructions made from a new projections”, IEEE Comp. Society(1973), 275-285

GORDON, R. ; “A tutorial on ART”, IEEE Transactions on Science 21(1974), 78-93

HERMAN, G.T. ; “Reconstruction of Binary Patterns from a New Projection”, International Computing Symposium, Davos, Switzerland, North Holland Publ. Co.(1973), 371-379.

HOUNSFIELD, G. N. ; “Computerized Transverse Axial Scanning (Tomography) I: Description of System” , Brit. J. Radiol. 46 (1973), 1016-1022 .

HOUNSFIELD,G.N., “A method of and apparatus for examination of a body by radiation such as X or γ radiation”, British patent nro. 1283915, London. Issued to EMI Ltd Application filed Aug. 1968.

RADON, J. ; “On the determination of functions from their integrals along certain manifolds”, Ber. Saechs. Akad. Wiss, Leipzig Math. Phys. 69 (1917), 262-277.

VAZ, C. M. P., CRUVINEL, P. E., CRESTANA, S. , REICHARDT, K., STOLF, R.,“Using Computed Tomography Miniscanner for studing Tillage Induced Soil Compactation”, Soil Tecnology 21(1989),313-321.

HENDEE, Willian R., “The Physical Principles of Computed tomography ”, Little Brown and Company, Boston, 1983.